Published in final edited form as:
Cancer Discov. 2013 June ; 3(6): 636–647. doi:10.1158/2159-8290.CD-13-0050.

Identification of Targetable FGFR Gene Fusions in Diverse Cancers

Yi-Mi Wu[1,2], **Fengyun Su**[1,2], **Shanker Kalyana-Sundaram**[1,2], **Nick Khazanov**[3], **Bushra Ateeq**[1,2], **Xuhong Cao**[1,4], **Robert J. Lonigro**[1,5], **Pankaj Vats**[1,2], **Rui Wang**[1,2], **Su-Fang Lin**[6], **Ann-Joy Cheng**[7], **Lakshmi P. Kunju**[1,2], **Javed Siddiqui**[1,2], **Scott A. Tomlins**[1,2], **Peter Wyngaard**[3], **Seth Sadis**[3], **Sameek Roychowdhury**[1,8], **Maha H. Hussain**[8], **Felix Y. Feng**[1,5,9], **Mark M. Zalupski**[5,8], **Moshe Talpaz**[8], **Kenneth J. Pienta**[1,5,8,10], **Daniel R. Rhodes**[1,2,3,11], **Dan R. Robinson**[1,2,#], and **Arul M. Chinnaiyan**[1,2,4,5,10,12,#]

[1]Michigan Center for Translational Pathology, University of Michigan Medical School, Ann Arbor, MI 48109, USA

[2]Department of Pathology, University of Michigan Medical School, Ann Arbor, MI 48109, USA

[3]Compendia Bioscience, 110 Miller Avenue, Ann Arbor, MI 48104, USA

[4]Howard Hughes Medical Institute, University of Michigan Medical School, Ann Arbor, MI 48109, USA

[5]Comprehensive Cancer Center, University of Michigan Medical School, Ann Arbor, MI 48109, USA

[6]National Institute of Cancer Research, National Health Research Institutes, Miaoli County, Taiwan

[7]Department of Medical Biotechnology and Laboratory Science, Chang Gung University, Taiwan

[8]Department of Internal Medicine, University of Michigan Medical School, Ann Arbor, MI 48109, USA

[9]Depment of Radiation Oncology, University of Michigan Medical School, Ann Arbor, MI 48109, USA

[10]Department of Urology, University of Michigan Medical School, Ann Arbor, MI 48109 USA

[11]Department of Computational Medicine and Bioinformatics, University of Michigan Medical School, Ann Arbor, MI 48109, USA

[12]Center for Computational Medicine and Biology, University of Michigan, Ann Arbor, MI 48109, USA

Abstract

Through a prospective clinical sequencing program for advanced cancers, four index cases were identified which harbor gene rearrangements of *FGFR2* including patients with

[#]Corresponding Authors: Arul M. Chinnaiyan, M.D., Ph.D., Director, Michigan Center for Translational Pathology, Investigator, Howard Hughes Medical Institute, S. P. Hicks Endowed Professor of Pathology, American Cancer Society Professor, Professor of Urology, University of Michigan Medical School, 1400 E. Medical Center Dr. 5316 CCGC, Ann Arbor, MI 48109-5940, arul@umich.edu. Dan R. Robinson, Ph.D., Research Assistant Professor, Michigan Center for Translational Pathology, 1400 E. Medical Center Dr. 5410 CCGC, Ann Arbor, MI 48109-5940, danrobi@umich.edu.

Disclosure of Potential Conflicts Of Interest

A.M.C. is a consultant to Life Technologies, co-founder of Compendia Biosciences, which is now owned by Life Technologies, and advisor to Ventana/Roche and Gen-Probe/Hologic.

cholangiocarcinoma, breast cancer, and prostate cancer. After extending our assessment of FGFR rearrangements across multiple tumor cohorts, we identified additional FGFR gene fusions with intact kinase domains in lung squamous cell cancer, bladder cancer, thyroid cancer, oral cancer, glioblastoma, and head and neck squamous cell cancer. All FGFR fusion partners tested exhibit oligomerization capability, suggesting a shared mode of kinase activation. Overexpression of FGFR fusion proteins induced cell proliferation. Two bladder cancer cell lines that harbor FGFR3 fusion proteins exhibited enhanced susceptibility to pharmacologic inhibition *in vitro* and *in vivo.* Due to the combinatorial possibilities of FGFR family fusion to a variety of oligomerization partners, clinical sequencing efforts which incorporate transcriptome analysis for gene fusions are poised to identify rare, targetable FGFR fusions across diverse cancer types.

Keywords

MI-ONCOSEQ; integrative clinical sequencing; FGFR fusions; driver mutations; therapeutic targets

INTRODUCTION

Advances in next-generation sequencing technologies have refined the molecular taxonomy of a spectrum of human diseases and facilitated a move towards “precision medicine” (1, 2). With regards to oncology, defining the mutational landscape of an individual patient’s tumor will lead to more precise treatment and management of cancer patients. Comprehensive clinical sequencing programs for cancer patients have been initiated at a variety of medical centers including our own (3, 4). In addition to the potential of identifying “actionable” therapeutic targets in cancer patients, these clinical sequencing efforts may lead to the identification of novel “driver” mutations that may be rare in a common cancer type or be newly revealed in relatively rare cancer types.

Recurrent gene fusions are an important class of “driver mutation” in cancer as exemplified by the *BCR-ABL* gene fusion which characterizes chronic myeloid leukemia (CML) (5). Importantly, virtually all CML patients harbor the BCR-ABL kinase fusion and respond to the small molecule kinase inhibitor, imatinib, representing one of the earliest examples of precision medicine in practice (6). In 2005, it was discovered that over 50% of prostate cancers harbor recurrent gene fusions of the androgen-regulated gene *TMPRSS2* with ETS transcription factors (7), suggesting that gene fusions/translocations may play a significant role in common epithelial tumors similar to hematologic malignancies and sarcomas. Subsequently, recurrent gene rearrangements have been identified in carcinomas of the lung, breast, colon, and thyroid, among other epithelial tissues (8–12). Of these, the *EML4-ALK* kinase gene fusion, which characterizes 1–5% of lung adenocarcinomas, has gained the most traction in the context of precision therapy-- as patients with this gene fusion respond to the kinase inhibitor crizotinib (13, 14). Recently, *FGFR1* and *FGFR3* fusions with *TACC1* and *TACC3*, respectively, have been identified in approximately 3% of the tumor glioblastoma multiforme (GBM) (15) and *FGFR3-TACC3* fusions were identified in a subset of bladder carcinomas (16). Pre-clinical studies suggest that GBM patients with FGFR-TACC gene fusions may benefit from targeted FGFR kinase inhibition (17, 18).

RESULTS

Our IRB approved clinical sequencing program, called MI-ONCOSEQ (the Michigan Oncology Sequencing Program), enrolls patients with advanced cancer across all histologies (3). Since April of 2011, we have enrolled over 100 patients on this program which involves obtaining a current tumor biopsy with matched normal samples (blood and/or buccal swab).

The samples are then subjected to integrative sequencing which includes whole exome sequencing of the tumor and matched normal, transcriptome sequencing, and as needed, low pass genome sequencing (3). This combination of DNA and RNA sequencing technologies allows one to be relatively comprehensive with regards to the mutational landscape of coding genes including point mutations, indels, amplifications, deletions, gene fusions/ translocations, and outlier gene expression. These results are generated within a 5 to 7 week time frame and are presented at an institutional “precision tumor board” (previously called sequencing tumor board) to deliberate upon potentially actionable findings.

In this study, four MI-ONCOSEQ patients were prospectively identified that harbored gene fusions of *FGFR2* by transcriptome sequencing (Fig. 1). The first patient (MO_1036) was a 34 year old female diagnosed with metastatic cholangiocarcinoma. By whole exome sequencing of the tumor relative to the matched normal we detected 8 nonsynonymous somatic point mutations (Supplementary Table S1). The most interesting of these in terms of tumor biology was the inactivation of the SWI/SNF chromatin remodeling complex through mutation of *ARID1A* (Q1573*) and *PBRM1* (C736*). The SWI/SNF complex has been implicated as a tumor suppressor and inactivating somatic mutations of *ARID1A* and *PBRM1* have been identified in renal cell carcinoma, breast, and ovarian cancer (19). The copy number landscape for MO_1036 as determined by whole exome sequencing is shown in Fig. 1A and Supplementary Table S2. Interestingly, by paired-end RNA sequencing we detected an intrachromosomal fusion which resulted in the in frame fusion of the *FGFR2* kinase to *BICC1* (Fig. 1A). While 7 additional chimeric RNAs were detected (Supplementary Table S3), only the *FGFR2-BICC1* fusion exhibited a combination of high supporting reads (n= 259), predicted in-frame fusion protein, and potential therapeutic actionability via kinase inhibition. The *FGFR2-BICC1* fusion was confirmed by Q-PCR analysis (Fig. 1A). Neither copy number aberrations nor point mutations were observed in *FGFR2* or *BICC1.*

The second MI-ONCOSEQ patient with an *FGFR2* fusion (MO_1039) was a 61 year old male with metastatic cholangiocarcinoma. Like the first patient, this individual’s tumor expressed an *FGFR2-BICC1* fusion of identical configuration (Fig. 1B, Supplementary Table S4). This fusion was similarly validated by Q-PCR (Fig. 1B). By contrast, however, this cholangiocarcinoma case exhibited 27 nonsynonymous somatic point mutations including an inactivating mutation of *TP53* (R267W, Supplementary Table S5) and a distinct copy number landscape (Fig. 1B, Supplementary Table S6). Neither point mutations nor copy number changes in FGFR genes were identified in this patient.

The third patient with an *FGFR2* fusion identified was a 31 year old woman with metastatic breast cancer (MO_1051). RNA sequencing revealed an in frame interchromosomal fusion of *FGFR2* with *AFF3* which had a functional structure analogous to the FGFR2 kinase fusions found in cholangiocarcinoma (Fig. 1C). In addition to the *FGFR2-AFF3* fusion, which was detected with 138 supporting reads and validated by Q-PCR (Fig. 1C), 6 additional gene fusions with a lower number of reads were identified (Supplementary Table S7). This breast cancer case also harbored 204 nonsynonymous point mutations including mutation of *TP53* (G199E) and a known activating mutation of *PIK3CA* (H1047R) (Supplementary Table S8). While this breast cancer case exhibited a number of amplifications and deletions (Supplementary Table S9), as expected (based on past clinical pathology data) this patient was negative for the *ERBB2* amplification.

The fourth patient (MO_1081) with an *FGFR2* fusion identified was a 57 year old male with Gleason score 5+4 metastatic prostate cancer. Transcriptome sequencing of a brain metastasis revealed an interchromosomal fusion of *SLC45A3* with *FGFR2* in which the *SLC45A3* non-coding exon 1 is fused to the intact coding region of *FGFR2* (Fig. 1D,

Supplementary Table S10). Since *SLC45A3* is a prostate-specific, androgen-regulated gene (20), the *SLC45A3-FGFR2* fusion is predicted to drive overexpression of wild type FGFR2. Importantly, FGFR2 exhibited outlier expression in the index case relative to our compendium of prostate cancer tissues (n=84; Fig. 1D), and a similar rare case of *FGFR2* outlier expression was identified in the Glinsky *et al* (21) prostate cancer cohort (Supplementary Fig. S1A and B).

As we had identified novel *FGFR2* gene fusions in cholangiocarcinoma, breast cancer and prostate cancer, we next asked whether FGFR family fusions are present across carcinomas of different histologies. To address this we analyzed RNA-seq data generated from an internal cohort of diverse tumors (n=322) and The Cancer Genome Atlas (TCGA) effort (n=2053) (Supplementary Table S11) for gene fusions using several bioinformatics approaches (See Methods). Including the initial 4 index cases, we identified 24 tumors or cell lines with *FGFR1*, *2*, and *3* fusions (Fig. 2, Supplementary Tables S12, S13, and S14). All of the gene fusions nominated expressed an FGFR family member as a 5′ or 3′ fusion partner with intact kinase domains suggesting potential actionability. 5′ FGFR fusions to *BICC1*, *AFF3*, *CASP7*, *CCDC6*, *KIAA1967*, *OFD1*, *BAIAP2L1* and *TACC3* (multiple exons) were identified and 3′ FGFR fusions to *SLC45A3*, *BAG4* and *ERLIN2* were identified. Cancer types harboring FGFR fusions were quite diverse and included cholangiocarcinoma (n=2), breast cancer (n=4), prostate cancer (n=1), thyroid cancer (n=1), lung squamous cell carcinoma (n=6), bladder cancer (n=5), oral cancer (n=1), head and neck squamous cell carcinoma (n=2), and glioblastoma (n=2). FGFRs are known to exhibit tissue-specific splicing, resulting in IIIb and IIIc isoforms (22). Both IIIb and IIIc isoforms of *FGFR2* and *FGFR3* were evident in the RNA-seq data of the fusion cases, depending on cancer type (Supplementary Table S12).

As most of the diverse FGFR fusion partners contribute domains with known dimerization motifs, including coiled-coil, SAM, LIS1, BAR, SPHF, and caspase (23–29), we hypothesized that oligomerization may serve as the common mechanism of activation of FGFR fusion proteins. Thus, we expressed selected epitope tagged versions of the FGFR fusions in HEK 293T cells and looked for protein oligomerization by co-immunoprecipitation. As examples, while FGFR3-BAIAP2L1, FGFR3-TACC3, FGFR2-BICC1, and FGFR2-CCDC6 interact *in vitro*, wild-type FGFR2 and FGFR3 do not in the absence of FGF ligands (Fig. 3A, Supplementary Fig. 2). We also show that the isolated fusion domains provided by BAIAP2L1, TACC3, KIAA1967, CCDC6, and BICC1 interact *in vitro* as oligomerization domains (Supplementary Fig. 3), further supporting the notion of oligomerization induced activation of FGFR kinase fusions. We additionally demonstrated dimerization capability of the colled-coli domain present in the FGFR2-CIT fusion identified recently in a lung adenocarcinoma by Seo *et al* (30) (Supplementary Fig. 3).

Unlike wild-type FGFR2 and FGFR3, overexpression of selected examples of FGFR fusions including FGFR2-BICC1, FGFR3-BAIAP2L1, and FGFR3-TACC3 in 293T cells induced morphological changes characterized by rounding up of cells (Supplementary Fig. S4). Overexpression of these FGFR fusion proteins also enhanced cell proliferation based on real-time cell imaging (Fig. 3B). To further demonstrate that FGFR fusion kinases are biologically active, we stably expressed FGFR fusions in benign immortalized TERT-HME cell lines. Stable lines harboring the FGFR3-BAIAP2L1, FGFR3-TACC3, and FGFR2-CCDC6 fusions showed expression of active FGFR fusion kinases (as demonstrated by tyrosine phosphorylation of the fusion kinases) and enhanced proliferation of the cells (Fig. 3C–E). Activation of downstream MAP kinase ERK1/2 and the transcription factor STAT1 was also observed in the stable lines (Supplementary Fig. S5). Additionally, the ERLIN2-FGFR1 fusion also produces an active FGFR kinase, as shown by tyrosine phosphorylation of the expressed fusion construct (Supplementary Fig. S6).

To evaluate the effects of pharmacologic inhibition of cells naturally harboring FGFR fusions, we assessed the sensitivity of bladder cancer cell lines to an FGFR small molecule kinase inhibitor PD173074(31). SW780 cells were characterized to have a fusion of *FGFR3-BAIAP2L1* in this study and Williams *et al.* (16) (Supplementary Fig. S7A), while J82 and HT-1197 cells harbor activating point mutations of *FGFR3* (K652E and S249C respectively(32), COSMIC). Importantly, while the FGFR fusion cell line SW780 was sensitive to nanomolar concentrations of PD173074, the FGFR3 mutant cell lines used here were not (Fig. 4A), suggesting that FGFR fusions may exhibit sensitivity to FGFR inhibitors, while some FGFR mutations are known to be resistant (33). Inhibition of proliferation was also demonstrated with a second FGFR inhibitor pazopanib, again showing sensitivity of the FGFR fusion positive lines SW780 and RT4 (Supplementary Fig. S7B). PD173074 exerted a cell cycle arrest effect on fusion positive SW780 cells, but not fusion-negative HT-1197 cells (Supplementary Fig. S8). Similar results for FGFR fusion-positive lines were obtained *in vivo*. SW780 xenografts exhibited decreased tumor growth with increasing doses of PD173074 while J82 xenografts did not (Fig. 4B). Expression of the *FGFR3-BAIAP2L1* fusion *in vitro* induces ERK1/2 activation (Supplementary Fig. S5) and similarly, fusion-positive SW780 xenografts exhibit strong ERK1/2 activation, which can be abolished by treatment with the FGFR inhibitor PD173074 (Fig. 4C). The RT4 urothelial carcinoma line harboring a *FGFR3-TACC3* fusion also exhibited sensitivity to FGFR inhibition in a xenograft model (Fig. 4B). Toxicity of PD173074 was monitored by assessment of mouse body weight (Supplementary Fig. 7C).

Further experiments utilizing siRNA knockdown demonstrate the central role of *FGFR3-BAIAP2L1* fusion in SW780 cell proliferation. Knockdowns using either *FGFR3* of *BAIAP2L1* siRNAs resulted in a dramatic reduction in cell proliferation in fusion-positive SW780 cells. In contrast, knockdown of *FGFR3* or *BAIAP2L1* did not have significant effects on cell proliferation in either fusion negative cell lines J82 or HT-1197 (Supplementary Fig. S9).

DISCUSSION

Sequencing and analysis of each of the four FGFR fusion patients described in this study were carried out in a time frame of 5 to 7 weeks. The sequencing results were each presented at our bi-monthly multi-disciplinary precision tumor board for discussion and deliberation. The first cholangiocarcinoma patient MO_1036, who harbored the *FGFR2-BICC1* fusion, underwent a conventional chemotherapy regimen in which her cancer progressed and chose not to pursue FGFR directed therapy and died 3 months after enrollment on this protocol. The second cholangiocarcinoma patient, MO_1039, also harboring an *FGFR2-BICC1* fusion underwent conventional chemotherapy but did not show tumor shrinkage and was enrolled on an FGFR inhibitor clinical trial. The metastatic breast cancer patient, MO_1051, harboring the *FGFR2-AFF3* fusion, died of end-stage disease before the sequencing results were available, while the metastatic prostate cancer patient underwent irradiation of the brain (after brain metastasis resection) and continues to be maintained on hormonal treatment. Due to his brain metastasis, the prostate cancer patient was not eligible for an FGFR clinical trial.

Activating point mutations of *FGFR1*, *FGFR2*, *FGFR3* or *FGFR4* have been identified in a variety of cancers including gliomas, bladder cancer, multiple myeloma, and rhabdomyosarcomas (34). Studies of hematological diseases led to the identification of 3′ gene fusions of *FGFR1* in myeloproliferative disorder (35) and 3′ *FGFR3* fusions in peripheral T-cell lymphoma (36) and multiple myeloma (35). As described earlier, 5′ gene fusions of *FGFR1* and *FGFR3* with *TACC1* and *TACC3* have recently been identified in GBM in two studies(15, 37). Here, we identify potentially actionable 5′ and 3′ FGFR

rearrangements across a diverse array of both common and rare solid tumors. Ten novel FGFR fusion partners were identified. In the Singh *et al* GBM study, the mechanism of activation of the FGFR fusions is proposed to be through mis-localization to mitotic spindle poles mediated by the coiled-coil domain of TACC fusion partner (15). This presumably leads to mitotic and chromosomal segregation defects triggering aneuploidy. In the Parker *et al* GBM study, increased expression through loss of the FGFR3 3′ UTR and miR-99a regulation is hypothesized as an activating mechanism (37). While these may be potential mechanisms in the specific case of the FGFR3-TACC3 fusion proteins in GBM, this likely does not explain the diverse array of fusion partners identified for FGFRs in this study. We propose a different, potentially more inclusive, model in which the FGFR fusion partners (e.g., *BICC1*, *TACC3*, *CCDC6*, *BAIAP2L1*, *KIAA1967*, *CASP7*, *CIT*, and *OFD1*) mediate oligomerization, which triggers activation of the respective FGFR kinase. Of note, we have not detected any FGFR fusions that result in simple truncation of the FGFR protein, despite prior investigations suggesting that 3′ truncating splicing isoforms encode activated FGFR2 proteins (38). The FGFR fusions detected have persistently exhibited substantial dimerization domain contributions from the 3′ fusion partner.

The *SLC45A3-FGFR2* gene fusion identified in the index prostate cancer is quite interesting as its pathogenic role is likely through a mechanism that is distinct from fusion protein oligomerization (shared by the other gene fusions tested). The entire open reading frame of *FGFR2* is expressed under the control of an androgen-regulated promoter of *SLC45A3*, leading to the marked overexpression of FGFR2. The *SLC45A3-FGFR2* fusion is analogous to the previously characterized *TMPRSS2-ETS* gene fusions characterized in over 50% of prostate cancers (7). One would predict that this patient should respond to second generation anti-androgens, such as MDV3100 (39), as well as FGFR inhibition. Another interesting observation in this study is the enhanced sensitivity to the FGFR inhibitor PD173074 of cell lines harboring an *FGFR3* fusion relative to those that have an activating point mutation of *FGFR3*. While beyond the scope of this study, additional FGFR inhibitors and larger panels of FGFR fusions and FGFR mutant cell lines will need to be studied to determine the broader applicability of these results. Clinical trials for several FGFR inhibitors are underway or in late stage pre-clinical development (33, 40, 41). It will be important to enrich these early stage clinical trials with patients harboring FGFR gene fusions similar to the successful development of the small molecule kinase inhibitor crizotonib in lung cancer patients harboring the *EML4-ALK* gene fusion. The wide range of cancers in which FGFR rearrangements were detected in this study, suggest that development of FGFR rearrangements are lineage independent and emphasizes the importance of developing mutation enriched clinical trials rather than trials based on tissue of origin. While each individual type of genetic aberration may occur at low frequency, the integrated sequencing approach identifies a wide range of informative genetic aberrations, potentially guiding the enrollment into numerous trials of diverse therapeutics.

In this study, we identified 4 patients with FGFR family gene fusions through an established clinical sequencing project called MI-ONCOSEQ (the Michigan Oncology Sequencing Program). Combining these index patients with an analysis of transcriptome data from our internal tumor cohorts as well as the TCGA identified FGFR fusions in a wide array of cancers including cholangiocarcinoma, GBM, squamous lung cancer, bladder cancer, breast cancer, thyroid cancer, oral cancer, head and neck squamous cell carcinoma, and prostate cancer. In addition to *TACC1* and *TACC3*, we identified 10 additional FGFR fusion partners as well as implicated 3 out 4 FGFR family members (*FGFR1*, *2*, and *3*) in gene rearrangements. We also suggest a common mechanism of activation of these fusion proteins and show that FGFR gene fusion positive cancers have enhanced susceptibility to FGFR inhibitors over activating point mutations of FGFR.

METHODS

Clinical Study and specimen collection

Sequencing of clinical samples was performed under Institutional Review Board (IRB)–approved studies at the University of Michigan. Patients were enrolled and consented for integrative tumor sequencing, MI-ONCOSEQ (Michigan Oncology Sequencing Protocol, IRB# HUM00046018)(3). Medically qualified patients 18 years or older with advanced or refractory cancer are eligible for the study. Informed consent details the risks of integrative sequencing and includes up-front genetic counseling. Biopsies were arranged for safely accessible tumor sites. Needle biopsies were snap frozen in OCT and a longitudinal section was cut. Hematoxylin and eosin (H&E) stained frozen sections were reviewed by pathologists to identify cores with highest tumor content. Remaining portions of each needle biopsy core were retained for nucleic acid extraction.

Cell lines and antibodies

Cell lines were purchased from the American Type Culture Collection (ATCC) and verified by next-generation transcriptome sequencing methods to identify known somatic mutations (COSMIC database). Oral cancer cell lines were obtained from their originating lab (A.J.C.), and are not verified. Cells were grown in specified media supplemented with fetal bovine serum and antibiotics (Invitrogen). Anti-c-Myc antibody was purchased from Sigma. Anti-V5 antibody was purchased from Life Technologies. Anti-FGFR3 antibodies were purchased from Epitomics and Cell Signaling. Antisera for phospho-FGFR, phospho-ERK1/2, pan-ERK1/2, phospho-STAT1, and pan-STAT1 were purchased from Cell Signaling. Anti-phosphotyrosine antibody clone 4G10 is from Millipore.

DNA/RNA isolation and cDNA synthesis

Genomic DNA from frozen needle biopsies and blood was isolated using the Qiagen DNeasy Blood & Tissue Kit, according to the manufacturer's instructions. Total RNA was extracted from frozen needle biopsies using the Qiazol reagent with disruption using a 5mm bead on a Tissuelyser II (Qiagen), and purified using a miRNeasy kit (Qiagen) with DNase I digestion, according to the manufacturer's instructions. Total RNA was isolated from cancer cell lines using the Trizol reagent (Life Technologies). RNA integrity was verified on an Agilent 2100 Bioanalyzer using RNA Nano reagents (Agilent Technologies). cDNA was synthesized from total RNA using SuperScript III (Invitrogen) and random primers (Invitrogen) for quantitative RT-PCR analysis.

Preparation of next generation sequencing libraries

Transcriptome libraries were prepared following Illumina's TruSeq RNA protocol, using 1–2μg of total RNA. Poly(A)$^+$ RNA was isolated using Sera-Mag oligo(dT) beads (Thermo Scientific) and fragmented with the Ambion Fragmentation Reagents kit (Ambion, Austin, TX). cDNA synthesis, end-repair, A-base addition, and ligation of the Illumina indexed adapters were performed according to Illumina's protocol. Libraries were size-selected for 250–300 bp cDNA fragments on a 3% Nusieve 3:1 (Lonza) agarose gel, recovered using QIAEX II gel extraction reagents (Qiagen), and PCR-amplified using Phusion DNA polymerase (New England Biolabs) for 14 PCR cycles. The amplified libraries were purified using AMPure XP beads. Library quality was measured on an Agilent 2100 Bioanalyzer for product size and concentration. Paired-end libraries were sequenced with the Illumina HiSeq 2000, (2×100 nucleotide read length). Reads that passed the chastity filter of Illumina BaseCall software were used for subsequent analysis.

Exome libraries of matched pairs of tumor/normal genomic DNAs were generated using the Illumina TruSeq DNA Sample Prep Kit, following the manufacturer's instructions. 3 μg of

each genomic DNA was sheared using a Covaris S2 to a peak target size of 250 bp. Fragmented DNA was concentrated using AMPure XP beads (Beckman Coulter), followed by end-repair, A-base addition, and ligation of the Illumina indexed adapters according to Illumina's protocol. The adapter-ligated libraries were electrophoresed on 3% Nusieve 3:1 (Lonza) agarose gels and fragments between 300 to 350 bp were recovered using QIAEX II gel extraction reagents (Qiagen). Recovered DNA was amplified using Illumina index primers for 8 cycles. The amplified libraries were purified using AMPure XP beads and the DNA concentration was determined using a Nanodrop spectrophotometer. 1 μg of the libraries were hybridized to the Agilent SureSelect Human All Exon V4 at 65°C for 60 hr following the manufacturer's protocol (Agilent). The targeted exon fragments were captured on Dynal M-280 streptavidin beads (Invitrogen), and enriched by amplification with the Illumina index primers for 9 additional cycles. After purification of the PCR products with AMPure XP beads, the quality and quantity of the resulting exome libraries were analyzed using an Agilent 2100 Bioanalyzer and DNA 1000 reagents.

We used the publicly available software FastQC to assess sequencing quality. For each lane, we examine per-base quality scores across the length of the reads. Lanes were deemed passing if the per-base quality score boxplot indicated that >75% of the reads had >Q20 for bases 1–80. In addition to the raw sequence quality, we also assess alignment quality using the Picard package. This allows monitoring of duplication rates and chimeric reads that may result from ligation artifacts; crucial statistics for interpreting the results of copy number and structural variant analysis.

Nomination of gene fusions

To identify gene fusions, paired-end transcriptome reads passing filter were mapped to the human reference genome and UCSC genes, allowing up to two mismatches, with Illumina ELAND software (Efficient Alignment of Nucleotide Databases) and Bowtie (42). Sequence alignments were subsequently processed to nominate gene fusions using the method described earlier (9). In brief, paired end reads were processed to identify those that either contained or spanned a fusion junction. Encompassing paired reads refer to those in which each read aligns to an independent transcript, thereby encompassing the fusion junction. Spanning mate pairs refer to those in which one sequence read aligns to a gene and its paired-end spans the fusion junction. Both categories undergo a series of filtering steps to remove false positives before being merged together to generate the final chimera nominations. Reads supporting each fusion were realigned using BLAT (UCSC Genome Browser) to reconfirm the fusion breakpoint.

Mutation Analyses

We annotated the resulting somatic mutations using RefSeq transcripts. HUGO gene names were used. The impact of coding non-synonymous amino acid substitutions on the structure and function of a protein was assessed using BLOSUM scores. We also assessed whether the somatic variant was previously reported in dbSNP135 or COSMIC v5668.

Tumor content for each tumor exome library was estimated from the sequence data by fitting a binomial mixture model with two components to the set of most likely SNV candidates on 2-copy genomic regions. The set of candidates used for estimation consisted of coding variants that (1) exhibited at least 3 variant fragments in the tumor sample, (2) exhibited zero variant fragments in the matched benign sample with at least 16 fragments of coverage, (3) were not present in dbSNP, (4) were within a targeted exon or within 100 base pairs of a targeted exon, (5) were not in homopolymer runs of four or more bases, and (6) exhibited no evidence of amplification or deletion. In order to filter out regions of possible amplification or deletion, we used exon coverage ratios to infer copy number changes, as

described below. Resulting SNV candidates were not used for estimation of tumor content if the segmented log-ratio exceeded 0.2 in absolute value. Candidates on the Y chromosome were also eliminated because they were unlikely to exist in 2-copy genomic regions. Using this set of candidates, we fit a binomial mixture model with two components using the R package flexmix, version 2.3–8. One component consisted of SNV candidates with very low variant fractions, presumably resulting from recurrent sequencing errors and other artifacts. The other component, consisting of the likely set of true SNVs, was informative of tumor content in the tumor sample. Specifically, under the assumption that most or all of the observed SNV candidates in this component are heterozygous SNVs, we expect the estimated binomial proportion of this component to represent one-half of the proportion of tumor cells in the sample. Thus, the estimated binomial proportion as obtained from the mixture model was doubled to obtain an estimate of tumor content.

Copy number aberrations were quantified and reported for each gene as the segmented normalized log2-transformed exon coverage ratios between each tumor sample and matched normal sample (43). To account for observed associations between coverage ratios and variation in GC content across the genome, lowess normalization was used to correct per-exon coverage ratios prior to segmentation analysis. Specifically, mean GC percentage was computed for each targeted region, and a lowess curve was fit to the scatterplot of log2-coverage ratios vs. mean GC content across the targeted exome using the lowess function in R (version 2.13.1) with smoothing parameter f=0.05.

Somatic point mutations were identified in the tumor exome sequence data using the matched normal exome data to eliminate germline polymorphisms. Parameters and computational methods were as previously described (44).

For RNA-Seq gene expression analysis, transcriptome data was processed as previously described. Genes were nominated as exhibiting potential “outlier” expression relative to a cohort of N=282 previously sequenced tissues using the following conditions: (1) the gene was required to have an expression value of at least 20 RPKM in the sample of interest; (2) the gene was required to be at or above the 90th percentile relative to all previously sequenced tissues, of any type; (3) the gene was required to have a fold change of at least 2 relative to the maximum RPKM over all previously sequenced benign tissues; and (4) the 25th percentile of the gene expression measurements over the previously sequenced tissues was required to be less than 50 RPKM. Collectively, these parameters target genes with (1) high absolute expression, (2) high expression relative to previously sequenced tissues, (3) high expression relative to all benign tissues, and (4) expression that is not uniformly high across all tissues.

Partially redundant sequencing of areas of the genome affords the ability for cross validation of findings. We cross-validated exome-based point mutation calls by manually examining the genomic and transcriptomic reads covering the mutation using the UCSC Genome Browser. Likewise, gene fusion calls from the transcriptome data can be further supported by structural variant detection in the genomic sequence data, as well as copy number information derived from the genome and exome sequencing.

Quantitative RT-PCR

For validation of fusion transcripts, quantitative RT-PCR assays were performed. Total cDNAs of index cases and negative control samples were synthesized using SuperScript III System according to the manufacturer’s instructions (Invitrogen). Quantitative RT-PCR was performed using fusion-specific primers (Supplementary Table 15) with SYBR Green Master Mix (Applied Biosystems) on the StepOne Real-Time PCR System (Applied Biosystems). The PCR products were further analyzed by agarose gel electrophoresis.

Relative mRNA levels of the fusion transcripts were normalized to the expression of the housekeeping gene *GAPDH*.

Inhibition of FGFR receptors and cell proliferation assay

Bladder cancer cells SW780, J82, and HT1197 were seeded into 96-well plates in triplicate and allowed to attach before drug treatment. The FGFR inhibitor PD173074 (Selleck Chemicals) was added to the cultures at concentrations of 0, 5, 25, and 100 nM. Relative cell numbers were measured by WST-1 assays at indicated time points following the manufacturer's instructions (Roche). To test the effects of the FGFR inhibitor pazopanib (Selleck Chemicals) on cell proliferation, SW780, RT4, J82, and HT-1197 cells were seeded into 24-well plates in quadruplicates and allowed to attach before drug treatment. Pazopanib was added to the cultures at concentrations of 0, 0.1, 0.5, and 1 μM. Cell proliferation was determined by IncuCyte live-cell imaging system (Essen Biosciences).

Cloning and expression of FGFR fusions

The FGFR fusion alleles were PCR amplified from cDNA of the index cases or cell lines using the primers listed in the Supplementary Table 15 and the Expand High Fidelity protocol (Roche). PCR products were digested with restriction endonuclease and ligated into the pcDNA3.1 vector (Invitrogen), which had been modified to contain a C-terminal MYC-epitope tag or V5-epitope tag. Expression constructs were transfected into HEK 293T cells using FuGene HD transfection reagent (Promega). Cells were harvested 24-hours post-transfection for protein analysis. For stable line establishment in TERT-HME cells, FGFR fusion alleles were cloned into the pCDH510B lentiviral vector (System Biosciences), which had been modified to contain a C-terminal V5 epitope tag. Lentiviruses were produced with the ViraPower packaging mix (Invitrogen) in 293T cells using FuGene HD transfection reagent (Roche). Benign TERT-HME cells at 30% confluence were infected at an MOI of 20 with the addition of polybrene at 8 mg/ml, and the cells were selected by 20 μg/ml puromycin. Stable pools of resistant cells were obtained and analyzed for expression of the FGFR fusion proteins by western blot analysis with anti-V5 antibody. Cell proliferation was measured by IncuCyte imaging system as described above.

For the cell proliferation assay, HEK 293T cells were transfected with control vector or FGFR fusion constructs. Twenty-four hours post-transfection, cells were trypsinized, resuspended in DMEM medium containing 2% FBS, and plated in quadruplicate at 12,000 cells per well in 24 well plates. The plates were incubated at 37°C and 5% CO2 atmosphere using the IncuCyte live-cell imaging system (Essen Biosciences). Cell proliferation was assessed by kinetic imaging confluence measurements at 3-hour time intervals.

Co-immunoprecipitation

HEK 293T cells were grown to ~70% confluence in DMEM supplemented with 10% fetal bovine serum, followed by transfection with MYC-tagged or V5-tagged expression construct alone, or in combination using FuGene6 reagent (Promega). Twenty-four hours after transfection, cell pellets were lysed in lysis buffer (58 mM Na2HPO4, 17 mM NaH2PO4, 68 mM NaCl, 1% Triton X-100, 0.5% sodium deoxycholate, 0.1% SDS, and protease inhibitors), followed by immunoprecipitation with tag epitope-specific antibodies (Sigma) and protein-G Dynabeads (Invitrogen). Precipitates were washed three times with IP Wash buffer (20 mM Tris, pH8, 2 mM EDTA, 150mM NaCl, 1% Triton X100) and eluted in SDS-PAGE loading buffer at 95°C for 5 min. Immuno-precipitated proteins were separated on SDS-PAGE and detected by Western blotting with tag epitope-specific antibodies (Sigma).

siRNA knockdown of *FGFR3* and *BAIAP2L1*

SW780, J82, and and HT-1197 bladder cancer cells were transfected twice with FGFR3-targeting siRNA, BAIAP2L1-targeting siRNA, or non-targeting siRNA (Thermo Scintific Dharmacon) using DharmaFECT1 reagent (Dharmacon). The siRNAs used were as follows: ON-TARGETplus FGFR3 L-003133-00-0005, ON-TARGETplus BAIAP2L1 L-018664-00-0005, and ON-TARGETplus Non-targeting pool. Twenty-four hours after transfection, cells were trypsinized and plated in triplicate at 8,000 cells per well in 24-well plates. The plates were incubated at 37°C with 5% CO2 atmosphere in the IncuCyte live-cell imaging system (Essen Biosciences). Cell proliferation rate was assessed by kinetic imaging confluence measurements at 3-hour time intervals.

Mouse Xenograft Models

Five week-old male C.B17/SCID mice were procured from a breeding colony at University of Michigan, maintained by Dr. Kenneth Pienta. Mice were anesthetized using a cocktail of xylazine (80 mg/kg, intraperitoneal) and ketamine (10 mg/kg, intraperitoneal) for chemical restraint. Bladder cancer cells SW780 (2 million cells for each implantation site) or J82 (5 million cells for each implantation site) were resuspended in 100 μl of 1XPBS with 20% Matrigel (BD Biosciences) and were implanted subcutaneously into flank region on both sides. Eight mice were included in each experimental group. All tumors were staged for two weeks (SW780 cells) and three weeks (J82 cells) before starting the drug treatment. Xenografted mice with palpable tumors were treated with a FGFR inhibitor PD173074 (Selleck Chemicals) dissolved in 5% ethanol in corn oil (intraperitoneal). Mice in control group received 5% ethanol in corn oil as vehicle control. Tumor growth was recorded weekly by using digital calipers and tumor volumes were calculated using the formula (π/6) (L×W2), where L= length of tumor and W= width. Any decrease in the body weight of mice was monitored bi-weekly during the course of the study. All experimental procedures involving mice were approved by the University Committee on Use and Care of Animals (UCUCA) at the University of Michigan and conform to their relevant regulatory standards. Tumor tissues from xenografted SW780 cells were harvested and lysed in RIPA buffer containing protease/phosphatase inhibitors for Western blot analysis.

Supplementary Material

Refer to Web version on PubMed Central for supplementary material.

Acknowledgments

Financial support

This project is supported in part by the Prostate Cancer Foundation, the NCI Early Detection Research Network (U01 CA111275), NIH RO1CA132874-01, a Department of Defense Era of Hope Scholar Award, and the University of Michigan Comprehensive Cancer Center Prostate SPORE (P50CA 069568). A.M.C. is supported by a Stand Up To Cancer -Prostate Cancer Foundation Prostate Dream Team Translational Cancer Research Grant. Stand Up To Cancer is a program of the Entertainment Industry Foundation administered by the American Association for Cancer Research (SU2C-AACR-DT0712). A.M.C. is also supported by the Alfred A. Taubman Institute, the American Cancer Society, the Howard Hughes Medical Institute, and a Doris Duke Charitable Foundation Clinical Scientist Award.

The authors thank Terrance Barrette and Doug Gibbs for hardware and database management, Shanda Birkeland, Mary Pierce-Burlingame and Karen Giles for assistance with sample and manuscript preparation, Rachell Stender for animal care and Dan Hayes for referral of patients to the MI-ONCOSEQ program. We also thank the larger MI-ONCOSEQ team including clinical research coordinator Lynda Hodges, Amy Gursky for patient sample procurement, cancer geneticists S. Gruber, J. Innis, bioethicists J. Scott Roberts and Scott Y. Kim, genetic counselors, J. Everett, J. Long and V. Raymond and radiologists, E. Higgins, E. Caoili, and R. Dunnick.

References

1. Chin L, Andersen JN, Futreal PA. Cancer genomics: from discovery science to personalized medicine. Nat Med. 2011; 17:297–303. [PubMed: 21383744]
2. Meyerson M, Gabriel S, Getz G. Advances in understanding cancer genomes through second-generation sequencing. Nat Rev Genet. 2010; 11:685–96. [PubMed: 20847746]
3. Roychowdhury S, Iyer MK, Robinson DR, Lonigro RJ, Wu YM, Cao X, et al. Personalized oncology through integrative high-throughput sequencing: a pilot study. Sci Transl Med. 2011; 3:111ra21.
4. Welch JS, Westervelt P, Ding L, Larson DE, Klco JM, Kulkarni S, et al. Use of whole-genome sequencing to diagnose a cryptic fusion oncogene. JAMA. 2011; 305:1577–84. [PubMed: 21505136]
5. Rowley JD. Letter: A new consistent chromosomal abnormality in chronic myelogenous leukaemia identified by quinacrine fluorescence and Giemsa staining. Nature. 1973; 243:290–3. [PubMed: 4126434]
6. Druker BJ. Translation of the Philadelphia chromosome into therapy for CML. Blood. 2008; 112:4808–17. [PubMed: 19064740]
7. Tomlins SA, Rhodes DR, Perner S, Dhanasekaran SM, Mehra R, Sun XW, et al. Recurrent fusion of TMPRSS2 and ETS transcription factor genes in prostate cancer. Science. 2005; 310:644–8. [PubMed: 16254181]
8. Perner S, Wagner PL, Demichelis F, Mehra R, Lafargue CJ, Moss BJ, et al. EML4-ALK fusion lung cancer: a rare acquired event. Neoplasia. 2008; 10:298–302. [PubMed: 18320074]
9. Robinson DR, Kalyana-Sundaram S, Wu YM, Shankar S, Cao X, Ateeq B, et al. Functionally recurrent rearrangements of the MAST kinase and Notch gene families in breast cancer. Nat Med. 2011; 17:1646–51. [PubMed: 22101766]
10. Santoro M, Melillo RM, Fusco A. RET/PTC activation in papillary thyroid carcinoma: European Journal of Endocrinology Prize Lecture. Eur J Endocrinol. 2006; 155:645–53. [PubMed: 17062879]
11. Seshagiri S, Stawiski EW, Durinck S, Modrusan Z, Storm EE, Conboy CB, et al. Recurrent R-spondin fusions in colon cancer. Nature. 2012; 488:660–4. [PubMed: 22895193]
12. Soda M, Choi YL, Enomoto M, Takada S, Yamashita Y, Ishikawa S, et al. Identification of the transforming EML4-ALK fusion gene in non-small-cell lung cancer. Nature. 2007; 448:561–6. [PubMed: 17625570]
13. Gerber DE, Minna JD. ALK inhibition for non-small cell lung cancer: from discovery to therapy in record time. Cancer Cell. 2010; 18:548–51. [PubMed: 21156280]
14. Kwak EL, Bang YJ, Camidge DR, Shaw AT, Solomon B, Maki RG, et al. Anaplastic lymphoma kinase inhibition in non-small-cell lung cancer. N Engl J Med. 2010; 363:1693–703. [PubMed: 20979469]
15. Singh D, Chan JM, Zoppoli P, Niola F, Sullivan R, Castano A, et al. Transforming fusions of FGFR and TACC genes in human glioblastoma. Science. 2012; 337:1231–5. [PubMed: 22837387]
16. Williams SV, Hurst CD, Knowles MA. Oncogenic FGFR3 gene fusions in bladder cancer. Hum Mol Genet. 2012
17. Lamont FR, Tomlinson DC, Cooper PA, Shnyder SD, Chester JD, Knowles MA. Small molecule FGF receptor inhibitors block FGFR-dependent urothelial carcinoma growth in vitro and in vivo. Br J Cancer. 2011; 104:75–82. [PubMed: 21119661]
18. Liang G, Liu Z, Wu J, Cai Y, Li X. Anticancer molecules targeting fibroblast growth factor receptors. Trends Pharmacol Sci. 2012; 33:531–41. [PubMed: 22884522]
19. Wilson BG, Roberts CW. SWI/SNF nucleosome remodellers and cancer. Nat Rev Cancer. 2011; 11:481–92. [PubMed: 21654818]
20. Tomlins SA, Laxman B, Dhanasekaran SM, Helgeson BE, Cao X, Morris DS, et al. Distinct classes of chromosomal rearrangements create oncogenic ETS gene fusions in prostate cancer. Nature. 2007; 448:595–9. [PubMed: 17671502]

21. Glinsky GV, Glinskii AB, Stephenson AJ, Hoffman RM, Gerald WL. Gene expression profiling predicts clinical outcome of prostate cancer. J Clin Invest. 2004; 113:913–23. [PubMed: 15067324]
22. Turner N, Grose R. Fibroblast growth factor signalling: from development to cancer. Nat Rev Cancer. 2010; 10:116–29. [PubMed: 20094046]
23. Browman DT, Hoegg MB, Robbins SM. The SPFH domain-containing proteins: more than lipid raft markers. Trends Cell Biol. 2007; 17:394–402. [PubMed: 17766116]
24. Chai J, Wu Q, Shiozaki E, Srinivasula SM, Alnemri ES, Shi Y. Crystal structure of a procaspase-7 zymogen: mechanisms of activation and substrate binding. Cell. 2001; 107:399–407. [PubMed: 11701129]
25. Ishizaki T, Naito M, Fujisawa K, Maekawa M, Watanabe N, Saito Y, et al. p160ROCK, a Rho-associated coiled-coil forming protein kinase, works downstream of Rho and induces focal adhesions. FEBS Lett. 1997; 404:118–24. [PubMed: 9119047]
26. Knight MJ, Leettola C, Gingery M, Li H, Bowie JU. A human sterile alpha motif domain polymerizome. Protein Sci. 2011; 20:1697–706. [PubMed: 21805519]
27. Mateja A, Cierpicki T, Paduch M, Derewenda ZS, Otlewski J. The dimerization mechanism of LIS1 and its implication for proteins containing the LisH motif. J Mol Biol. 2006; 357:621–31. [PubMed: 16445939]
28. Peter BJ, Kent HM, Mills IG, Vallis Y, Butler PJ, Evans PR, et al. BAR domains as sensors of membrane curvature: the amphiphysin BAR structure. Science. 2004; 303:495–9. [PubMed: 14645856]
29. Tong Q, Li Y, Smanik PA, Fithian LJ, Xing S, Mazzaferri EL, et al. Characterization of the promoter region and oligomerization domain of H4 (D10S170), a gene frequently rearranged with the ret proto-oncogene. Oncogene. 1995; 10:1781–7. [PubMed: 7753554]
30. Seo JS, Ju YS, Lee WC, Shin JY, Lee JK, Bleazard T, et al. The transcriptional landscape and mutational profile of lung adenocarcinoma. Genome Res. 2012; 22:2109–19. [PubMed: 22975805]
31. Mohammadi M, Froum S, Hamby JM, Schroeder MC, Panek RL, Lu GH, et al. Crystal structure of an angiogenesis inhibitor bound to the FGF receptor tyrosine kinase domain. EMBO J. 1998; 17:5896–904. [PubMed: 9774334]
32. Miyake M, Ishii M, Koyama N, Kawashima K, Kodama T, Anai S, et al. 1-tert-butyl-3-[6-(3,5-dimethoxy-phenyl)-2-(4-diethylamino-butylamino)-pyrido[2,3 -d]pyrimidin-7-yl]-urea (PD173074), a selective tyrosine kinase inhibitor of fibroblast growth factor receptor-3 (FGFR3), inhibits cell proliferation of bladder cancer carrying the FGFR3 gene mutation along with up-regulation of p27/Kip1 and G1/G0 arrest. J Pharmacol Exp Ther. 2010; 332:795–802. [PubMed: 19955487]
33. Guagnano V, Kauffmann A, Wohrle S, Stamm C, Ito M, Barys L, et al. FGFR genetic alterations predict for sensitivity to NVP-BGJ398, a selective pan-FGFR inhibitor. Cancer Discov. 2012
34. Wesche J, Haglund K, Haugsten EM. Fibroblast growth factors and their receptors in cancer. Biochem J. 2011; 437:199–213. [PubMed: 21711248]
35. Jackson CC, Medeiros LJ, Miranda RN. 8p11 myeloproliferative syndrome: a review. Hum Pathol. 2010; 41:461–76. [PubMed: 20226962]
36. Yagasaki F, Wakao D, Yokoyama Y, Uchida Y, Murohashi I, Kayano H, et al. Fusion of ETV6 to fibroblast growth factor receptor 3 in peripheral T-cell lymphoma with a t(4;12)(p16; p13) chromosomal translocation. Cancer Res. 2001; 61:8371–4. [PubMed: 11731410]
37. Parker BC, Annala MJ, Cogdell DE, Granberg KJ, Sun Y, Ji P, et al. The tumorigenic FGFR3-TACC3 gene fusion escapes miR-99a regulation in glioblastoma. J Clin Invest. 2013
38. Cha JY, Maddileti S, Mitin N, Harden TK, Der CJ. Aberrant receptor internalization and enhanced FRS2-dependent signaling contribute to the transforming activity of the fibroblast growth factor receptor 2 IIIb C3 isoform. J Biol Chem. 2009; 284:6227–40. [PubMed: 19103595]
39. Scher HI, Beer TM, Higano CS, Anand A, Taplin ME, Efstathiou E, et al. Antitumour activity of MDV3100 in castration-resistant prostate cancer: a phase 1–2 study. Lancet. 2010; 375:1437–46. [PubMed: 20398925]
40. Brooks AN, Kilgour E, Smith PD. Molecular pathways: fibroblast growth factor signaling: a new therapeutic opportunity in cancer. Clin Cancer Res. 2012; 18:1855–62. [PubMed: 22388515]

41. Greulich H, Pollock PM. Targeting mutant fibroblast growth factor receptors in cancer. Trends Mol Med. 2011; 17:283–92. [PubMed: 21367659]

42. Langmead B. Aligning short sequencing reads with Bowtie. Curr Protoc Bioinformatics. 2010; Chapter 11(Unit 11):7. [PubMed: 21154709]

43. Lonigro RJ, Grasso CS, Robinson DR, Jing X, Wu YM, Cao X, et al. Detection of somatic copy number alterations in cancer using targeted exome capture sequencing. Neoplasia. 2011; 13:1019–25. [PubMed: 22131877]

44. Grasso CS, Wu YM, Robinson DR, Cao X, Dhanasekaran SM, Khan AP, et al. The mutational landscape of lethal castration-resistant prostate cancer. Nature. 2012; 487:239–43. [PubMed: 22722839]

SIGNIFICANCE

High-throughput sequencing technologies facilitate defining the mutational landscape of human cancers, which will lead to more precise treatment of cancer patients. Here through integrative sequencing efforts, we identified a variety of FGFR gene fusions in a spectrum of human cancers. FGFR fusions are active kinases. Cells harboring FGFR fusions showed enhanced sensitivity to the FGFR inhibitors PD173074 and pazopanib, suggesting cancer patients with FGFR fusions may benefit from targeted FGFR kinase inhibition.

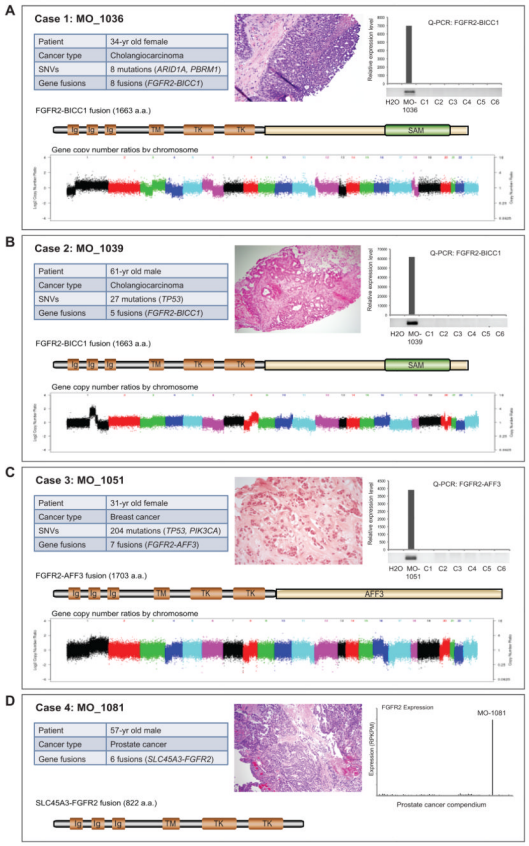

Figure 1. Integrative sequencing and mutational analysis of four index cancer patients found to harbor FGFR fusions

A CT-guided biopsy was employed to obtain tumor specimens from cancer patients enrolled in the MI-ONCOSEQ protocol. A sample of their normal tissue (blood or buccal swab) was also obtained for germline studies. The samples were subjected to integrative sequencing and analyzed for mutations. For each patient, a diagram summarizing the cancer type, histopathology, number of nonsynonymous somatic point mutations and gene fusions detected, and gene copy number landscape is presented. The predicted structure of the FGFR fusion protein identified in each case is illustrated. FGFR gene fusions were validated by quantitative RT-PCR followed by gel electrophoresis or outlier expression assessed by RNA-seq is provided. The four index cases shown are **A**, MO_1036, cholangiocarcinoma, **B**, MO_1039, cholangiocarcinoma, **C**, MO_1051, breast cancer, and **D**, MO_1081, prostate cancer. QPCR results for each case are compared to a set of 6 cDNA controls from unrelated patient tumors (C1-C6). For the prostate cancer patient, an expression of *FGFR2* is shown (in RPKPM) relative to a compendium of 84 prostate cancer samples.

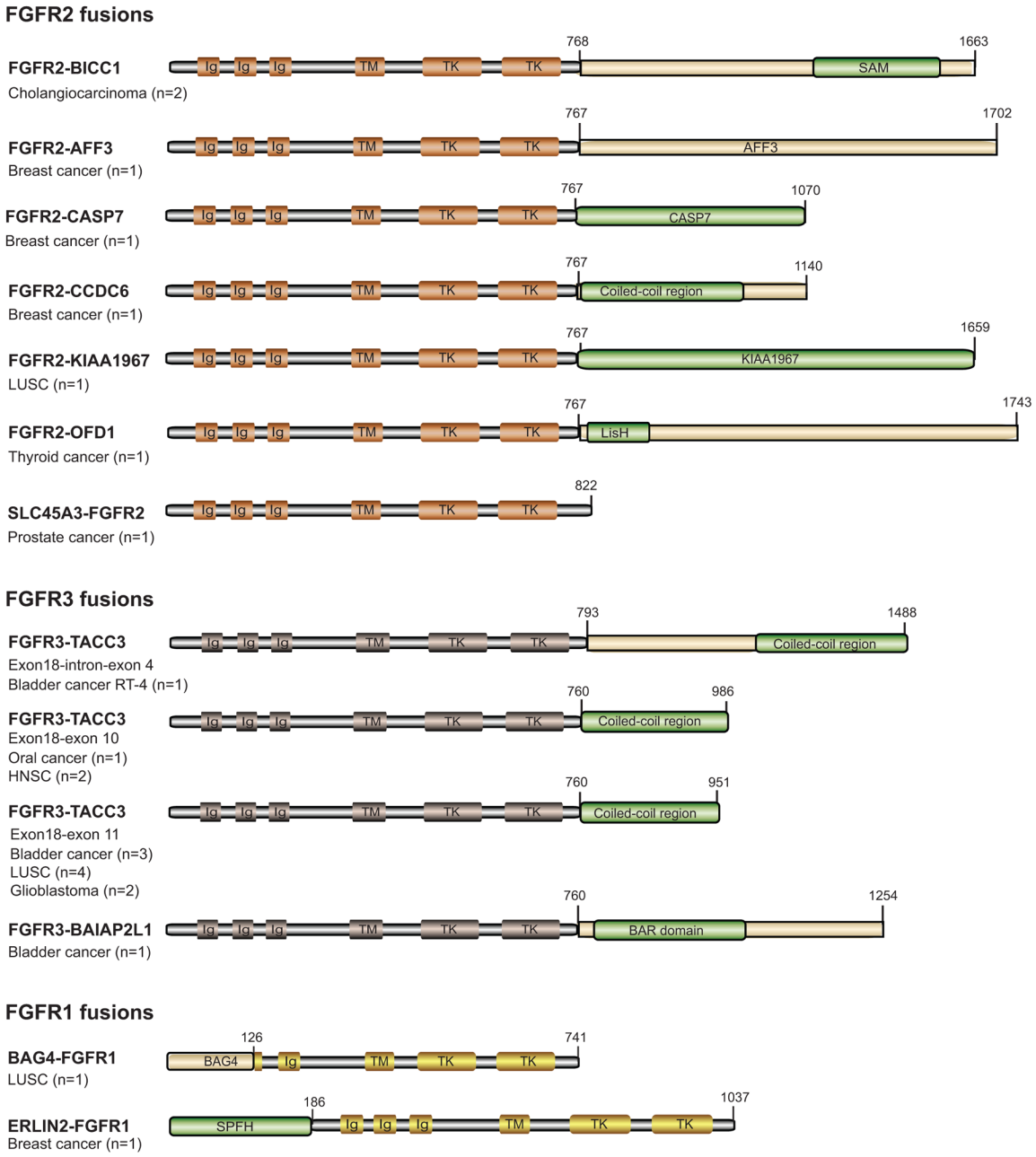

Figure 2. Schematic representations of the predicted FGFR gene fusions identified by transcriptome sequencing of human cancers

Data utilized includes RNA sequencing results from the 4 index patients, our internal tumor cohort and the TCGA compendium. Out of 4 FGFR receptor family members, *FGFR1*, *FGFR2*, and *FGFR3* are involved in gene fusions with various partners located on several chromosomes. Eleven distinct fusion partners of FGFRs were identified. Exon and codon numberings are based on the reference accessions in Supplementary Table 13. LUSC, Lung squamous cell carcinoma; HNSC, Head and Neck squamous cell carcinoma.

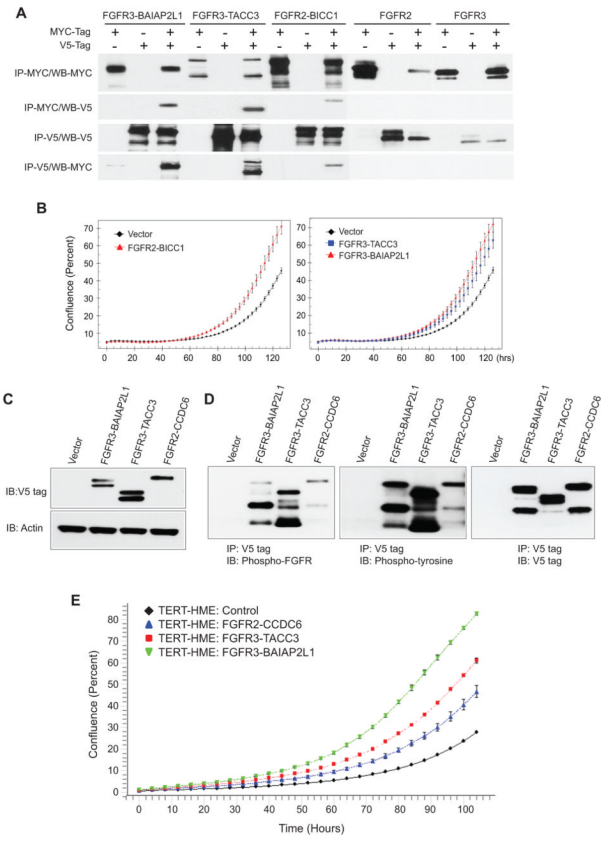

Figure 3. Functional characterization of FGFR fusion proteins

A, Oligomerization of FGFR fusion proteins demonstrated by immunoprecipitation (IP)-Western Blotting (WB). HEK 293T cells were transfected with respective Myc- and V5-tagged FGFR wild-type or fusion proteins and reciprocal IP-Western blots were carried out. **B**, Cell proliferation assays as determined by live-cell imaging of 293T cells over-expressing various FGFR fusion proteins. Data shown are cell confluence vs. time at 3 hour intervals. Each data point is the mean of quadruplicates. **C.** Stable expression of FGFR fusion proteins in TERT-HME cells. Cell lysates were prepared from various stable lines and expression of chimeric proteins was detected by anti-V5 antibody. **D**. FGFR fusion protein activity in TERT-HME cells. Cell lysates from various stable lines were immunoprecipitated (IP) and immunoblotted (IB) with the antibodies indicated. **E.** Overexpression of FGFR fusions induces cell proliferation in TERT-HME cells. Cell proliferation assays were performed by Incucyte live-cell imaging. Data shown are cell confluence vs. time at 3-hour intervals. Each data point is the mean of quadruplicates.

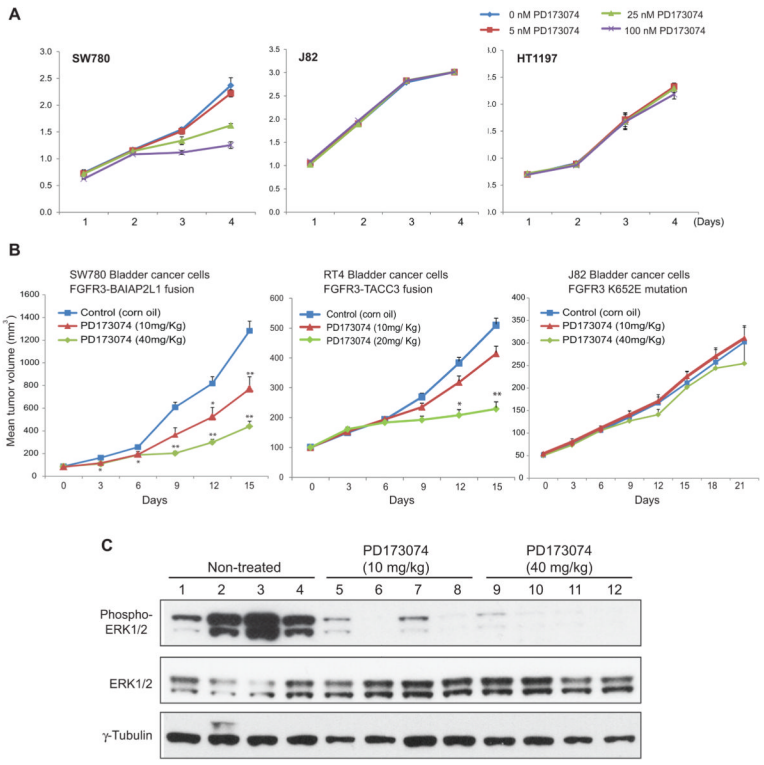

Figure 4. Inhibition of FGFR fusion kinase activity repressed tumor growth in a mouse xenograft model

A, Inhibition of cell proliferation by FGFR inhibitor PD173074. The *FGFR3-BAIAP2L1* bladder cell line SW780, and two control bladder cell lines J82 (K652E mutation) and HT-1197 (S249C mutation), were tested for the effects of PD173074 at three concentrations on cell proliferation, assessed by the WST-1 method at the indicated times. Data shown are the means of triplicates. **B**, Differential sensitivity of FGFR fusion positive versus FGFR mutant bladder cancer xenograft growth to PD173074. Mice xenografted with bladder cancer SW780 cells (*FGFR3-BAIAP2L1* fusion), RT4 (*FGFR3-TACC3* fusion), or J82 cells (K652E mutation) were treated daily with PD173074 after tumors were formed. The tumor size was monitored over a time course of 3 weeks. *p<0.05; **p<0.005. **C.** Inhibition of FGFR signaling pathway by FGFR inhibitor PD173074 in mouse xenograft tumors. Bladder cancer SW780 cells were implanted in mice and treated with PD173074 after tumor formation as shown in B. Protein lysates of tumor tissues were prepared and immunoblotted with antibodies against phospho-ERK1/2, pan-ERK1/2, and γ-tubulin.